Molecular Crystals and Liquid Crystals Incorporating Nonlinear Optics

Publication details, including instructions for authors and subscription information:
http://www.tandfonline.com/loi/gmcl17

Lateral Translational Diffusion and Electron Transport in Monolayer and Bilayer Assemblies of Amphiphiles at Interfaces

D. H. Charych [a], C. A. Goss [a], E. M. Landau [a] & M. Majda [a]

[a] Department of Chemistry, University of California - Berkeley, Berkeley, California, 94720

Version of record first published: 04 Oct 2006.

To cite this article: D. H. Charych , C. A. Goss , E. M. Landau & M. Majda (1990): Lateral Translational Diffusion and Electron Transport in Monolayer and Bilayer Assemblies of Amphiphiles at Interfaces, Molecular Crystals and Liquid Crystals Incorporating Nonlinear Optics, 190:1, 95-110

To link to this article: http://dx.doi.org/10.1080/00268949008047836

Mol. Cryst. Liq. Cryst., 1990, Vol. 190, pp. 95–110
Reprints available directly from the publisher
Photocopying permitted by license only

Printed in the United States of America

Lateral Translational Diffusion and Electron Transport in Monolayer and Bilayer Assemblies of Amphiphiles at Interfaces

D. H. CHARYCH, C. A. GOSS, E. M. LANDAU and M. MAJDA*

Department of Chemistry, University of California - Berkeley, Berkeley, California 94720

Two novel electrochemical methods of investigation of lateral processes in monolayer and bilayer assemblies are described. The first involves an interdigitated micro-electrode array consisting of fifty pairs of 50 nm thick, 800 nm long, and 4 μm wide electrodes deposited on a glass surface. An amphiphilic bilayer consisting in part of the N-methyl,N′-octadecylbipyridyl molecules is self-assembled in the inter-electrode gap. Translational diffusion of the electroactive amphiphile depends on the charge in the head group region and on the fluidity of the assembly controlled by the overall oxidation state of the octadecylbipyridyl. The second method involves 0.1 cm long, 50 nm wide gold micro-band electrodes positioned at the air/water interface and addressing surface monolayer of an octadecylferrocene amphiphile under controlled surface pressure conditions. Electrochemical measurements demonstrate that the lateral translational diffusion and the electron hopping involving ferrocene/ferrocenium sites are the two channels of the lateral charge transport.

INTRODUCTION

In this article, we give an overview of two electrochemical methods which our group has recently developed to study dynamics of lateral charge propagation in organized amphiphilic monolayer and bilayer assemblies. The first experimental approach is concerned with bilayer systems assembled at the solid/liquid interface. The second experiment involves Langmuir monolayers at the air/water interface. In both cases, the key element of our electrochemical measurements involves micro-electrodes positioned perpendicular to the monolayer assemblies. This characteristic feature of our experiments, shown schematically in Figure 1, allows us to relate current flow at the micro-electrode (under either steady-state - A, or transient - B conditions) to the rate of charge arrival at the electrode surface. Thus, we can probe the dynamics of lateral translational diffusion and lateral electron hopping involving the electro-active amphiphile in the monolayer assemblies. The discussion of these new techniques will be illustrated with a series of initial results.

Our interest in organized amphiphilic assemblies has several origins. One of these stems from their resemblance to biological membranes.[1] In such systems, membrane fluidity and dynamics of lateral processes are two of the fundamental

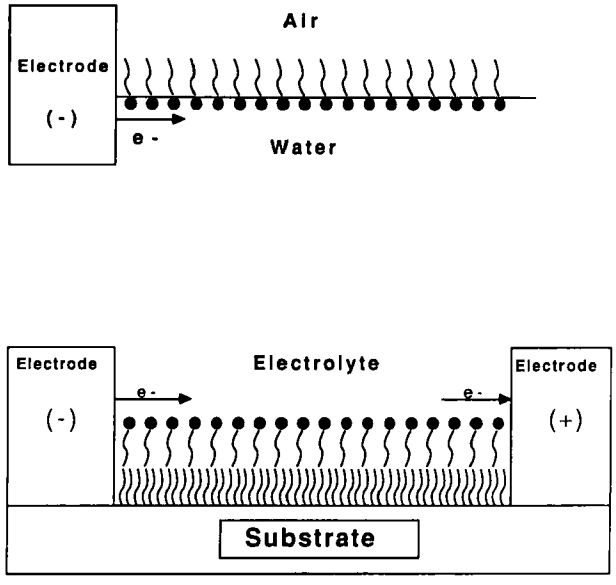

FIGURE 1 Schematic configuration of the micro-electrodes with respect to the monolayer and bilayer assemblies in the electrochemical measurements of the dynamics of lateral diffusion and charge transport.

phenomena responsible for many functions of cell membranes. Lateral diffusion of phospholipids has been measured using ESR[2] techniques as well as by monitoring recovery of photo-bleached fluorescence of a fluorescent label attached to a membrane component.[3] The latter technique has been used extensively in characterization of lipid and protein translational diffusion, phase transitions, and related phenomena in biological membrane systems. Several reviews on this subject are available in the literature.[4]

Concurrent with our own interest in biomimetic systems, we have been investigating the design of the catalytic assemblies at electrode surfaces in which amphiphilic bilayers provided structural order and directionality of charge transport.[5] An example of this type of system is shown in Figure 2. Here the bilayer assembly consists of an octadecyltrichlorosilane (OTS) monolayer, chemically bound to a microporous Al_2O_3 matrix, and a self-assembled monolayer of an octadecyl derivative of N-methyl-4,4′-bipyridyl ($C_{18}MV^{2+}$ octadecylviologen). Electrostatic interactions in the head group region of this monolayer account for a strong binding of ferricyanide ions, as shown. In this system, ferricyanide ions mediate oxidation of ascorbic acid at a potential *ca.* 300 mV less positive than the direct heterogeneous electro-oxidation of ascorbic acid.[5a] The $C_{18}MV^{2+}$ molecules are involved in a dynamic immobilization of the electrocatalyst, in that they provide also a means of its reoxidation via lateral transport from the individual hexacyanoferrate sites to the electrode surface. More thorough investigations of the dynamics of such lateral processes revealed that the hexacyanoferrate ions are engaged in diffusion along the head group region of the $C_{18}MV^{2+}$ monolayer by a kind of ion-hopping

$$2\,Fe(CN)_6^{3-} + H_2A \rightleftharpoons 2\,Fe(CN)_6^{4-} + A + 2H^+$$

$$Fe(CN)_6^{4-} - e \longrightarrow Fe(CN)_6^{3-}$$

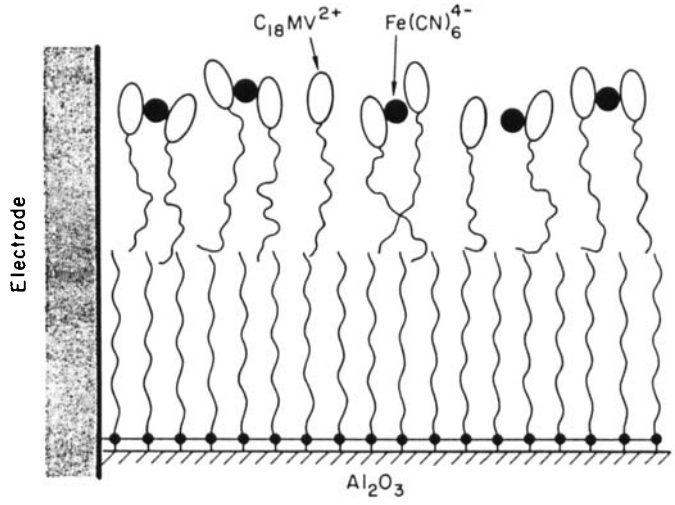

FIGURE 2 A schematic representation of the OTS/$C_{18}MV^{2+}$ bilayer assembly binding ferrocyanide ions which play the role of the mediator precursor in the catalytic electro-oxidation of ascorbic acid (H_2A) to ascorbate (A). The OTS monolayer is shown to be attached to the Al_2O_3 surface of a porous aluminum oxide film. The bilayer assembly is perpendicular to the electrode surface as a result of the perpendicular orientation of the microscopic pores of the oxide template.[9]

mechanism. More recently, we expanded our investigations to a similar electrocatalytic system in which a bilayer containing amphiphilic ferrocene molecules was involved in binding and electron transport mediation of glucose oxidase which supports electro-enzymatic oxidation of glucose.[5b]

Electrochemical investigations of the dynamics of lateral processes in OTS/$C_{18}MV^{2+}$ bilayers such as those in Figure 2 and single octadecylferrocene monolayers at the air/water interface are the subject of this report.

EXPERIMENTAL

Reagents

The synthesis and purification of N-methyl,N′-octadecyl-4,4′-bipyridyl chloride ($C_{18}MV^{2+}$) was described previously.[6] N-octadecylferrocenylamide ($C_{18}Fc$) was synthesized by reacting ferrocenecarboxylic acid chloride with octadecyl amine. The details of the synthesis and purification will be published elsewhere.[7] Octadecyltrichlorosilane (OTS) and 3-mercaptopropyltrimethoxysilane (MPTMS) were from Petrarch Systems Inc. OTS was vacuum distilled and stored in sealed ampules until just before use. Hexadecane was dried by passing it through a column of

activated neutral alumina just prior to use. Water was purified by passing house distilled water through Barnstead Nanopure II purification train. The resistivity of water used in the experiments was 18 Mohm cm or higher. All other chemicals were reagent grade and used as received.

Experimental procedures

The interdigitated arrays of micro-electrodes (IDA) were prepared in the Microfabrication Laboratory of the University of California at Berkeley in a class 100 clean room facility. Standard photo-lithographic procedures, similar to those outlined in the literature, were followed.[8] One important modification concerned the deposition of 50 nm gold films on glass substrates. The glass substrates were cleaned in 5:1 H_2O_2/conc. H_2SO_4 solution thermostated at 120°C for about 20 minutes and rinsed with water until the conductivity of the run off water was greater than 14 Mohm cm. Prior to gold vapor-deposition, the glass slides were coated with monolayer films of 3-mercaptopropyltrimethoxysilane. This was necessary to enhance adhesion of the gold films. The slides were immersed in a 2.5% (v:v) MPTMS solution in 2-propanol for 7 minutes, rinsed with 2-propanol, then cured at 100°C for 10 minutes. Immediately after the mercapto-silane treatment, the slides were placed in a Veeco Model 401 bell jar system equipped with a resistively heated thermal evaporation apparatus. Typically, the jar was evacuated to 2×20^{-7} Torr, then *ca.* 50 nm Au was coated at a rate of *ca.* 2 nm/s, at 10^{-6} Torr. The same coating procedure was used in the fabrication of the micro-band electrodes for the 2-D electrochemical experiments.

The self-assembly of the OTS and OTS/dibenzyldisulfide monolayers on glass and gold surfaces was similar to the previously established procedures.[9] The IDA electrodes were cleaned in chromic acid solution for 15–30 s, rinsed with H_2O for 60 s, immersed in 1:20 conc. HF/H_2O for 10 s, rinsed with H_2O for 60 s, then dried with a jet of Ar. The cleaned IDA substrates were placed in a hexadecane solution containing *ca.* 20 mM OTS and 1.5 mM dibenzyldisulfide for about 10 min. Upon removal the IDA electrodes were rinsed copiously with toluene and dried with Ar.

Instrumentation

The electrochemical experiments were carried out in the single compartment cells using a custom-designed micro-bipotentiostat and PAR instruments described previously. Langmuir monolayer films were investigated with a KSV Model 2000 trough equipped with a Wilhelmy-type film balance. The contact angle measurements were done with a Rame'-Hart Model 100 contact angle goniometer. A more detailed account of the instrumental procedures can be found elsewhere.[9]

RESULTS AND DISCUSSION

Steady-state charge transport in bilayer assemblies

We first present a steady-state electrochemical approach to the measurements of the dynamics of lateral charge transport processes in bilayer systems at the solid/

liquid interfaces. Our approach involves an interdigitated array of micro-electrodes (IDA) deposited on glass substrates using photo-lithographic techniques. The pattern of the micro-electrodes, shown schematically in Figure 3, consists of fifty pairs of 50 nm thick generator/collector electrodes, each of which is 800 μm long, 4 μm wide, and spaced by 4 μm.

Figure 3A shows a cross-section of a single generator/collector electrode pair in a bipotentiostatic circuit. Amphiphilic bilayers formed in a two step self-assembly procedure[9] are deposited on glass surfaces in the inter-electrode gap. Attached to the glass surface is an OTS monolayer. OTS also coats the surfaces of the gold micro-electrodes. To prevent electrode passivation, the self-assembly of OTS is carried out from OTS hexadecane solutions also containing dibenzyldisulfide (see Experimental Section). Dibenzyldisulfide competes with OTS for the sites on the gold surfaces and prevents their passivation. Since the disulfide has no affinity for the glass surface, the extent of organization of the OTS monolayers on glass is not perturbed by the presence of dibenzyldisulfide during the self-assembly procedure. The self-assembly of the second half of the bilayer is carried out in 300 μM $C_{18}MV^{2+}$,

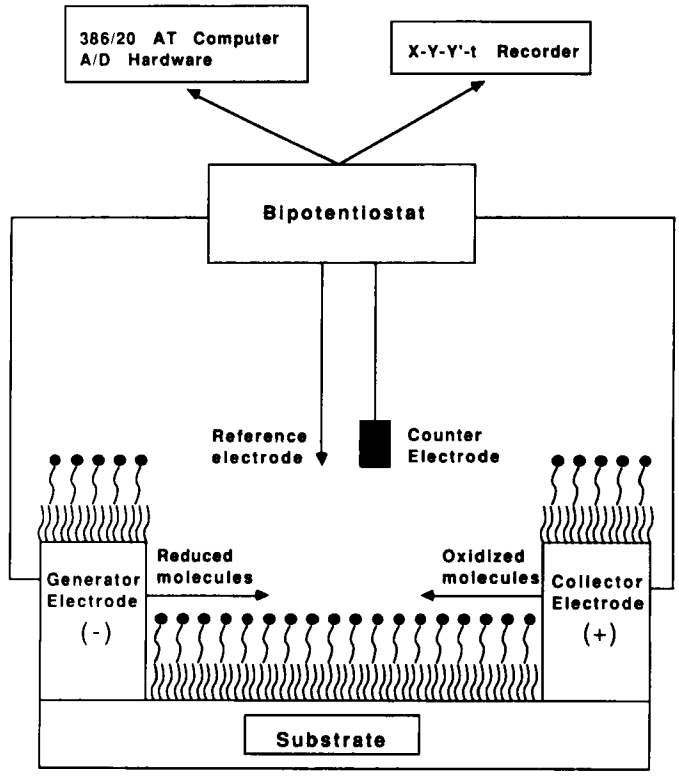

FIGURE 3 A schematic cross-sectional view of a single generator/collector pair of an interdigitated micro-electrode array in a bipotentiometric circuit used to study lateral charge transport in bilayer systems. The pattern of the micro-electrodes consists of fifty pairs of 50 nm thick generator/collector electrodes each of which is nominally 800 μm long, 4 μm wide, and is spaced by 4 μm.

0.5 M KCl solution for about 30 min. After removing the electrode, the loading solution was rinsed with 0.5 M KCl and transferred to deaerated 0.5 M KCl where all subsequent electrochemical measurements were done. This step also produces OTS/$C_{18}MV^{2+}$ bilayers on the surfaces of the micro-electrodes.

When the generator and collector electrodes of an IDA are connected together as a single working electrode, a potential scan produces current (Figure 4) characteristic for a system where all electroactive material is confined in a close proximity to the electrode surface. Since all the electroactive species present are reduced and then reoxidized, integration of the current in Figure 4 provides means for the coulometric determination of the $C_{18}MV^{2+}$ molecules in the bilayer assembly. A relatively slow potential scan of 20 mV/s was used to allow ample time for the $C_{18}MV^{2+}$ molecules in the inter-electrode gaps to diffuse along the bilayer assemblies to the micro-electrodes. When this experiment is done at a scan rate greater than *ca.* 20 V/s (50 V/s scans were used), only those octadecylviologen molecules assembled in bilayers on gold surfaces are addressed in the coulometric assay. A typical coverage of the $C_{11}MV^{2+}$ molecules, both in the OTS/$C_{18}MV^{2+}$ bilayer in the inter-electrode gap and those on gold surfaces, was the range $1.8 - 2.1 \times 10^{-10}$ mol/cm^2 (corrected for the roughness of the glass surface).

Consider now the generator-collector voltammetric experiment of Figure 5. The generator and collector micro-electrodes are initially potentiostated independently at the oxidizing potentials of 0.0 V and -0.2 V, respectively. The bipotentiostatic control of IDA allows us now to maintain the collector's potential at -0.2 V while the potential of the generator electrode is scanned first to -0.7 V and then back to 0.0 V. This generates collector current (Figure 5A) proportional to the rate of arrival of the $C_{18}MV^{+}$ produced at the generator electrode and diffusing across the inter-electrode gap. The observed histeresis is due to the time lag in the generation and detection of the reduced viologen amphiphile. When the same experiment is repeated with the initial potential set at -0.7 V, the current-voltage curve

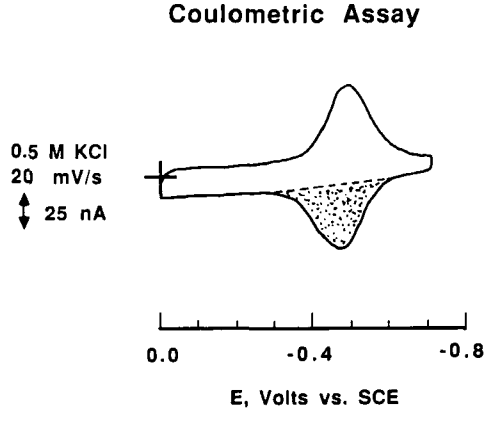

FIGURE 4 A current-voltage response of the $C_{18}MV^{2+}$/OTS bilayer assembled at an interdigitated micro-electrode array described in Figure 3. The generator and collector electrodes are driven at a common voltage as a single working electrode.

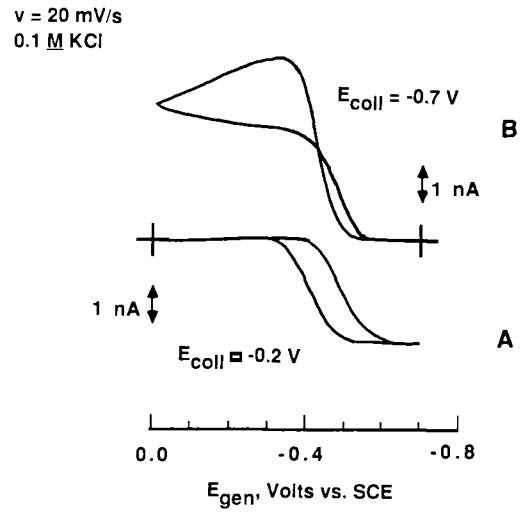

FIGURE 5 Generator-collector voltammetry of the $C_{18}MV^{2+}$/OTS bilayer assembled at an interdigitated micro-electrode array described in Figure 3. (**A**) E_{gen} is scanned from 0.0 V to −0.7 V and back to 0.0 V; E_{coll} = −0.2 V. (**B**) E_{gen} is scanned first from −0.7 V to 0.0 V and then back to −7 V; E_{coll} = −0.7 V.

in Figure 5B is obtained. The peak-shaped collector current is a result of fast diffusion of $C_{18}MV^{2+}$ along the bilayer which accounts for the transient component of the current response before the final steady-state is achieved. The comparison of the current responses in these two generator-collector experiments indicates the higher mobility of $C_{18}MV^{2+}$ than $C_{18}MV^{+}$ species. Differences between the diffusion coefficients of the two redox forms of the octadecyl viologen in favor of the doubly charged $C_{18}MV^{2+}$ were determined in our earlier experiments done under transient conditions.[9]

It is interesting to note that the limiting currents in Figure 5, achieved when the generator electrode is at −0.7 V (curve A) and 0.0 V (curve B), are equal, as one would expect for two sets of identical steady-state conditions. Since the same current is passed at the collector and generator electrodes, the flux of the $C_{18}MV^{2+}$ molecules to the cathode must be equal to the $C_{18}MV^{+}$ flux to the anode. Therefore, different concentration gradients of the two redox forms must develop across the inter-electrode gap to compensate for the differences in the diffusion coefficients of the reduced and oxidized viologen amphiphile. These steady-state conditions are shown schematically in Figure 6. The limiting steady-state current can be expressed in terms of Fick's first law:[10]

$$i_l = \frac{nF l \Gamma_t}{d}\left\{\frac{2D_o D_r}{D_o + D_r}\right\} \tag{1}$$

Here l is the total effective length of the collector (and generator) electrodes, Γ_t is the surface coverage of the viologen species in bilayer assemblies in the inter-

electrode gap, d is the width of the inter-electrode gap, and D_o and D_r are the diffusion coefficients of the oxidized and the reduced forms of the amphiphile, respectively.

The dependence of the limiting current in equation 1 on two diffusion coefficients does not allow one to deduce their individual values. To measure D_o and D_r independently, we sought to determine the concentration gradients of $C_{18}MV^{2+}$ and $C_{18}MV^{+}$ in Figure 6. To accomplish this, the concentrations of both forms of the viologen amphiphile at each micro-electrode were measured by fast scan (50 V/s) voltammetry. The knowledge of the concentration gradients enables us to interpret current under any steady-state conditions regardless of the value of the potential applied to the collector and generator electrodes. The advantage of this approach lies in its generality. Taking advantage of this capability, we carried out a series of experiments in which D_o and D_r were determined independently as a function of the overall ratio of the redox forms of the viologen amphiphile in the bilayer.

In these experiments, potential was applied to the collector and generator electrodes to establish certain steady-state conditions and the corresponding steady-state current was measured. At that point, fast scan voltammograms, initiated at the applied potential, were recorded at the collector and generator electrodes acting now as separate working electrodes. These experiments yield the coverages of $C_{18}MV^{2+}$ (O) and $C_{18}MV^{+}$ (R) at the anode ($\Gamma_{o,a}$ and $\Gamma_{r,a}$) and at the cathode ($\Gamma_{o,c}$ and $\Gamma_{r,c}$) for particular steady-state conditions. It can be shown that the limiting current can be now interpreted in terms of either of the following two equations:

$$i = \frac{n F l (\Gamma_{o,a} - \Gamma_{o,c}) D_o}{d} \tag{2}$$

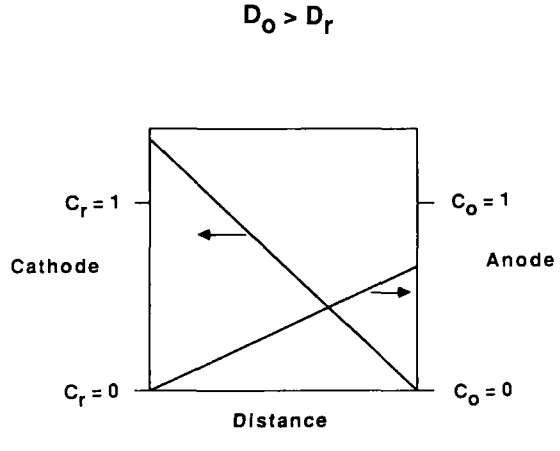

FIGURE 6 Schematic diagram of the concentration profiles of the oxidized (C_o) and reduced (C_r) forms of the octadecylviologen in the inter-electrode gap of an interdigitated micro-electrode array at the steady-state of Figure 5. The concentration levels marked $C_o = 1$ and $C_r = 1$ correspond to the initial concentrations of Figure 5A and 5B, respectively.

$$i = \frac{n F l (\Gamma_{r,c} - \Gamma_{r,a}) D_r}{d} \quad (3)$$

Analysis of Figure 6 leads to the realization that when the applied potential at the cathode and the anode is, respectively, completely reducing and oxidizing (i.e. the concentrations of O at the cathode and of R at the anode are equal to zero), then the overall ratio of the reduced to oxidized viologen species is significantly greater than unity. By controlling the potential of the cathode and the anode, we can control the O/R ratio of the viologen species in the inter-electrode gap.

Figure 7 presents the plots of D_o and D_r as a function of the mole fraction of R in the bilayer assembly. As mentioned above, $C_{18}MV^{2+}$ has a higher diffusion coefficient than its reduced form. At least two factors contribute to this effect. One is the electrostatic repulsion in the head group region which clearly induces higher mobility of the doubly charged viologen amphiphile. The second factor is the dimerization of the $C_{18}MV^{+}$ cation radicals. Combined with the lower charge of their head groups, this leads to partial aggregation of $C_{18}VM^{+}$ molecules. The most striking trend in Figure 7 is the strong dependence of D_o on the mole fraction of the reduced species. This decrease can be associated with the decrease of the overall fluidity of the monolayer assembly induced by less strongly charged $C_{18}MV^{+}$ molecules. Hence, it appears that the diffusion coefficient of $C_{18}MV^{2+}$ reflects both the extent of its interactions with the medium as well as characteristics of the medium itself. The relative independence of D_r of the monolayer composition suggests at least partial segregation of the reduced molecules into separate domains. Within these domains the molecules diffuse with a constant diffusion coefficient, independent of the monolayer composition. We have observed partial loss of elec-

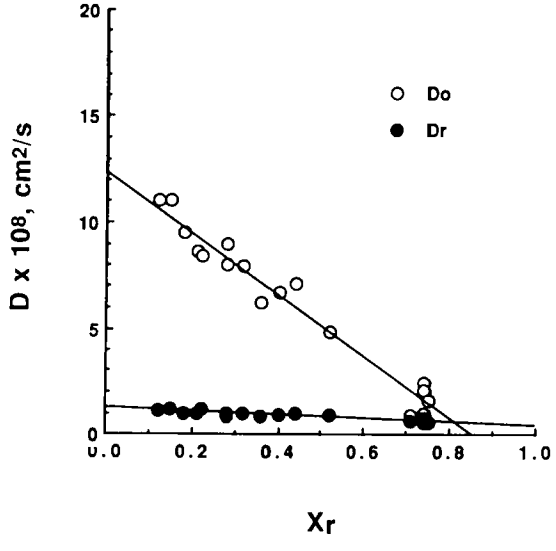

FIGURE 7 Plots of the lateral diffusion coefficients of $C_{18}MV^{2+}$ (D_o) and of $C_{18}MV^{+}$ (D_r) *vs.* the overall mole fraction of $C_{18}MV^{+}$ in the bilayer assembly in the inter-electrode gap of the array device.

troactivity when the bilayer assembly was held for several minutes in the reduced state.[9] This observation supports the notion of partial segregation of $C_{18}MV^+$. We postulate further that the presence of these domains is responsible for the decrease of the overall fluidity of the monolayer system.

Charge transport in Langmuir monolayers

The investigations of the translational diffusion in self-assembled monolayer assemblies described in the previous section suffer from a lack of precise control of the surface concentration of the electroactive amphiphile in the monolayer, and from partial instability of the self-assembled films over long periods of time. These deficiencies can be overcome by assembling monolayer systems at the air/water interface, where the control of the surface concentration is easily accomplished by sweeping the barrier of a Langmuir trough, and the stability of a monolayer is simply dictated by the insolubility of an amphiphile in the aqueous phase.

We have recently developed a novel electrochemical technique which allows investigation of the dynamics of lateral processes in Langmuir monolayers at the air/water interface.[11] The crucial elements of our experimental approach are shown in Figure 8. In the electrochemical experiments, the potential of the micro-band electrode positioned at the air/water interface is controlled by a three-electrode potentiostat. The counter and the reference electrodes are immersed in a subphase behind the barrier so that their presence does not interfere with Langmuir compressions of surface monolayers.

Fabrication of a working micro-band electrode, shown in Figure 8B, involves the following steps. A strip of gold *ca.* 2 cm long, 0.1 cm wide and 50 nm in thickness is vapor-deposited on a glass slide (*ca.* 1×2 cm^2). The entire surface of the glass slide with the deposited gold film is then coated with a C_{18}-alkyl monolayer by first exposing the glass slide to a solution of octadecylthiol, which is known to form well-ordered monolayers on gold surfaces.[12] In the second step, self-assembly of OTS on the glass surface is carried out as described in the experimental section. These steps render the glass and gold surfaces hydrophobic. The advancing contact angles with water measured both on the monolayer-coated glass and gold surfaces are in the range of 110°–112°. The actual preparation of a micro-band electrode involves breaking a gold-coated substrate along a line perpendicular to the gold strip, thus producing two electrodes with a freshly exposed, 50 nm wide, 0.1 cm long band of gold. An electrical contact is made on the face of the gold above the fracture line. When a micro-band electrode is positioned at the water surface as shown in Figure 8B, a three phase "interface" is formed along the line between the clean and the OTS-coated gold surface. Hence, molecules spread at the water surface are in contact with the a micro-band electrode along the three phase line.

The structure of an octadecylferrocene derivative ($C_{18}Fc$) investigated in these studies is shown in Figure 9. A room temperature surface pressure *vs.* area per molecule (π-A) isotherm recorded on pure water (Figure 9A) has a broad gas/liquid condensed (G/LC) coexistance region, followed by the steep compression of the condensed phase. The area per molecule obtained from this isotherm by extrapolation to $\pi = 0$ is 28 Å^2/molecule, suggesting a partial staggering of ferrocene

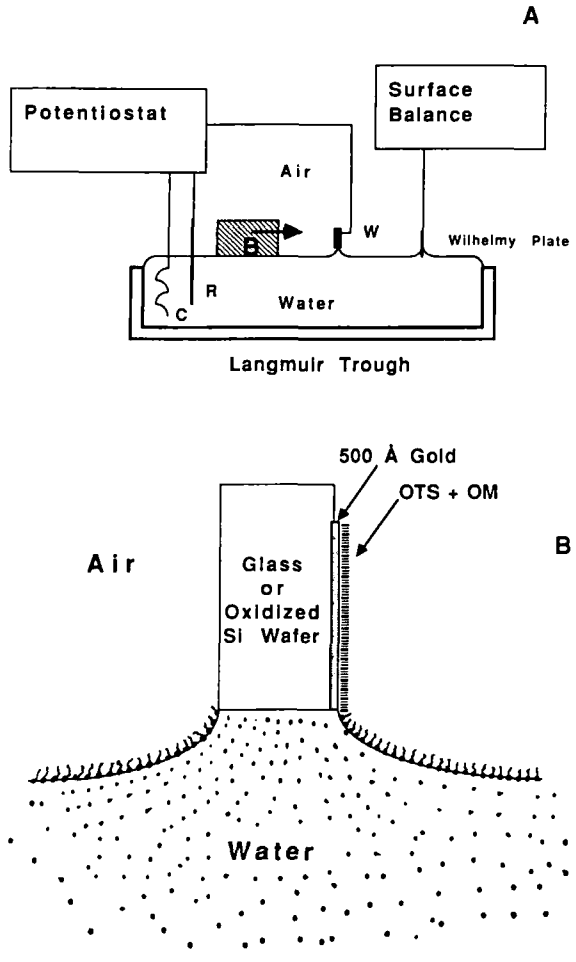

FIGURE 8 (**A**) A diagram of the essential elements of a 2-D electrochemical experiment. A Langmuir trough is equipped with a film balance and a movable barrier (**B**). A working micro-band electrode (W) is positioned at the air/water interface. The counter (C) and reference (R) electrodes are positioned behind the barrier so that their presence does not interfere with the surface monolayer and its compression. (**B**) A schematic cross sectional view of a micro-band electrode and its positioning at the air/water interface.

moieties in the head group region. Under these conditions of temperature and subphase composition, we were unable, so far, to observe electrochemical signal due to ferrocene oxidation. It appears that in the coexistance region the monolayer structure is dominated by the islands of a condensed phase, which are either non-electroactive or diffuse too slowly to produce measurable oxidation current in 2-D experiments.

The presence of perchloric acid (or $NaClO_4$) in the subphase, and higher temperature are two factors which contribute to dispersion of the condensed phase and stabilize, at least partially (see below), a fluid state of the monolayer. Under

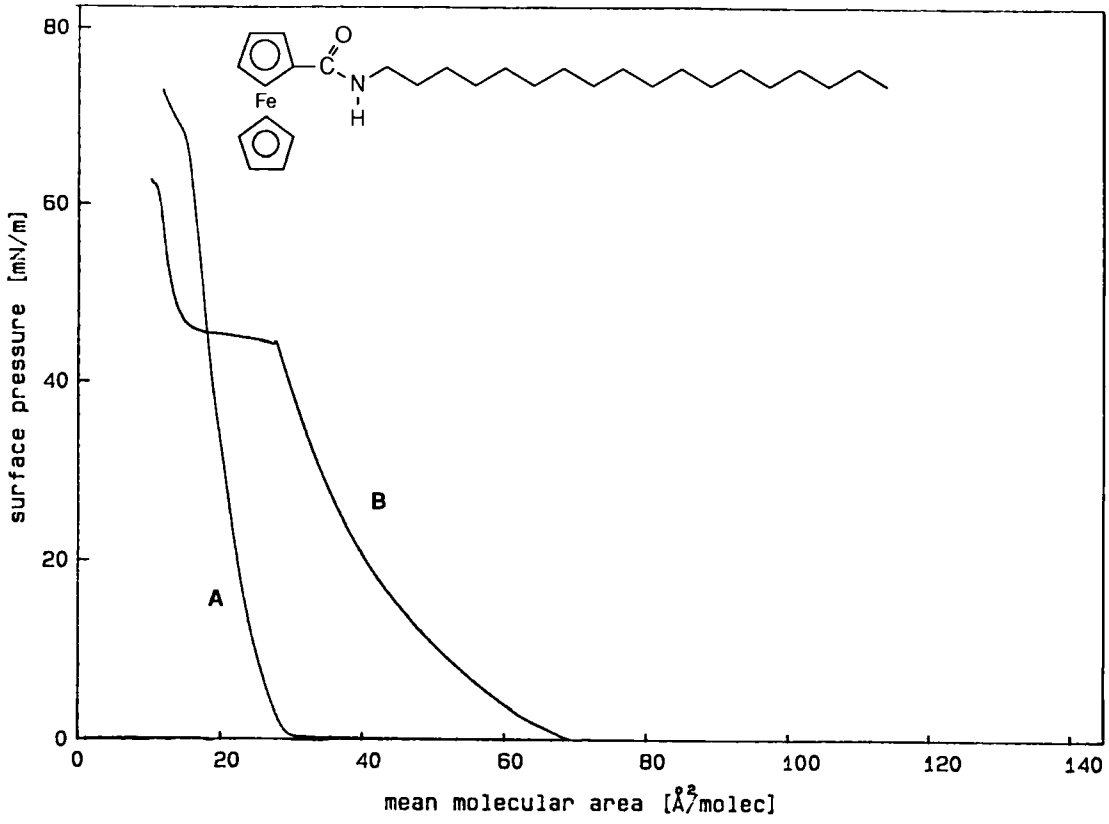

FIGURE 9 Surface pressure *vs.* area per molecule isotherms for the octadecylferrocene derivative shown in the figure. (A) pure aqueous subphase, T = 22.8°C. (B) 1.0 M $HClO_4$ subphase, T = 28.8°C.

these conditions (see isotherm B in Figure 9), an early pressure rise suggests that the region of $\pi = 0$ involves a fluid phase which, upon compression, undergoes a phase transition to the condensed phase at *ca.* 40 mN/m. The role of $HClO_4$ appears to involve its intercalation into the C_{18} Fc monolayer. A quasi-stable character of the fluid phase mentioned above is revealed by a small decrease of the area of the pressure on-set in isotherm B when the incubation time prior to compression is increased.

Fluidity of $C_{18}Fc$ monolayers seems to be a requirement of their electroactivity. When $C_{18}Fc$ monolayer is spread at any surface concentration below the LC phase transition on 1.0 M $HClO_4$ subphase at 30°C, one obtains well developed ferrocene cyclic voltammograms (i_p *ca.* 2 nA with a capacitive background level at *ca.* 50 pA at 200 mV/s), which match all criteria for a reversible, one-electron process at a planar electrode in a homogeneous solution.[13] The voltammetric peak current can be expressed by the following equation:

$$i_p = \text{const. } n^{3/2} v^{1/2} l \Gamma D^{1/2} \tag{4}$$

where v is the voltage scan rate, l is the electrode length, Γ is the surface concentration of $C_{18}Fc$, and D is its surface diffusion coefficient. It is worth noticing that the product of $l \times \Gamma$ in this equation is equivalent in terms of units to the usual product of $A \times C$, the electrode surface area and 3-D concentration. Thus, in the present case, the voltammetric current reflects dynamics of diffusional processes in surface monolayer obeying the linear diffusion equations.[13]

The stability of the voltammetric signal depends on the incubation time after monolayer spreading. The observed slow decrease of the voltammetric peak current is another sign of a quasi-stable character of the fluid phase observed on 1.0 M $HClO_4$. The decay of the peak currents with time is shown in Figure 10 for two initial $C_{18}Fc$ surface concentrations. The faster decay of the lower concentration monolayer could be explained in view of the postulated intercalation of $HClO_4$ into surface monolayers. The latter should be expected to be proportional to the $C_{18}Fc$ surface concentration. The data presented below were collected at *ca.* 1 min following monolayer spreading.

The diffusion coefficients of the lateral charge transport were obtained from the anodic peak current as a function of $C_{18}Fc$ surface concentration using equation 4. The data are plotted in Figure 11A. The initial decrease of the diffusion coefficient with increasing surface concentration can be understood in terms of the free volume model of Cohen and Turnbull.[14] They treated diffusion as a process which depends on density fluctuations around a diffusing molecule. Exchange of two neighboring molecules requires a free volume (here free area) greater or equal to a critical size v^* (here a^*). Their expression for diffusion coefficient transposed to a 2-D fluid system is:

$$D = D_o \exp [-a^*/a_f] \tag{5}$$

where $a_f = \bar{a} - a_o$, average free area per molecule ($\bar{a}$ and a_o are the average area occupied by a single molecule in the monolayer and the projected area of the

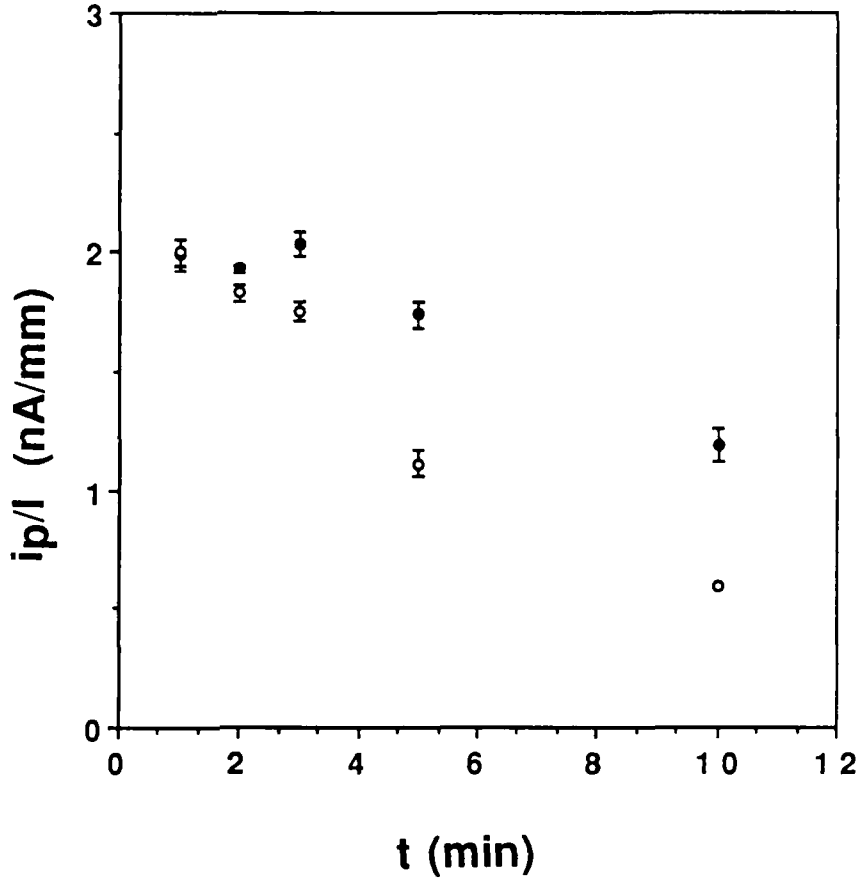

FIGURE 10 The effect of the incubation time following spreading of a $C_{18}Fc$ monolayer on the voltammetric signal (peak current normalized by the electrode length, i_p/l). Subphase—1.0 M $HClO_4$. Monolayer concentration: 120Å²/molecule—open circles, 300 Å²/molecule—closed circles. T = 29°C.

molecule itself). The logarithm plot of the data in Figure 11A according to equation 5 is given in Figure 11B. The best fit to the experimental data was obtained with a_o = 44 Å² which is in good agreement with the area per molecule obtained from the π-A isotherm (Figure 9B) by extrapolation to π = 0. A significant positive deviation in the experimental data above *ca.* 2.6 × 10^{-10} mol/cm² cannot be explained by any mechanism related to the physical motion of $C_{18}Fc$ in the monolayer. We postulate that these data indicate an onset of the second channel of the lateral electron transport involving electron hopping between the neighboring ferrocene/ferrocenium sites in the monolayer. We are currently investigating the surface concentration dependence of the apparent diffusion coefficient supported by electron hopping. Electrochemical data obtained in the low concentration limit should provide information concerning interfacial dynamics inaccessible by other techniques.

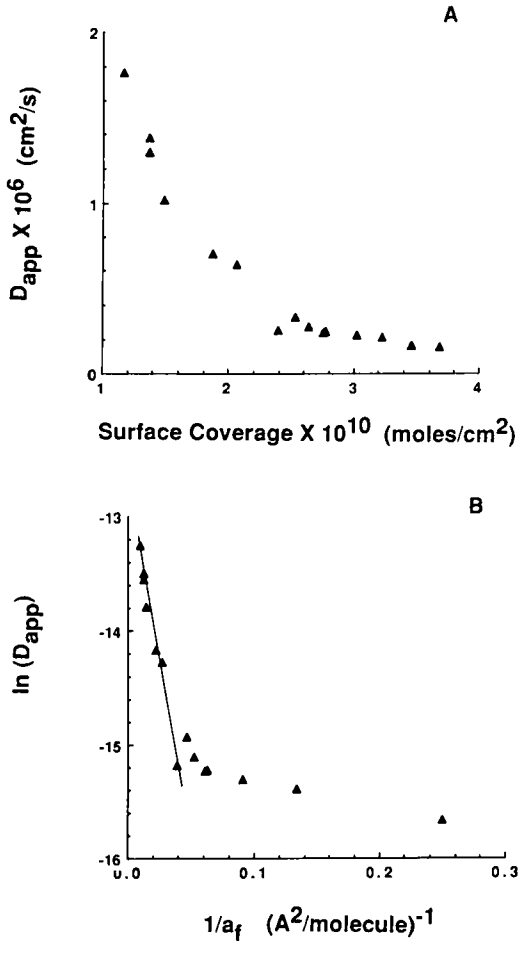

FIGURE 11 (**A**) A plot of the diffusion coefficient obtained from the 2-D voltammetric curves and equation 1 for the $C_{18}Fc$ monolayer on the 1.0 M $HClO_4$ subphase at 29°C. (**B**) A plot of the data in part A according to the free area model of diffusion in fluids (equation 5).

In conclusion, we have described two electrochemical approaches to the investigation of the dynamics of lateral processes in organized monolayer and bilayer assemblies. From the experimental point of view, both approaches involve design of micro-electrodes or integrated micro-electrode devices which can be positioned in perpendicular orientation to the monolayer assemblies. The data obtained thus far reveal that the translational diffusion depends not only on the structural features of the diffusing molecules, such as their charge, but that it also depends on the structure and characteristics of the entire assembly. Thus the techniques described here can provide information about microscopic fluidity of assemblies, phase transformations, self-segregation, electron transport, and other phenomena involving molecular assemblies as integrated entities.

Acknowledgments

We gratefully acknowledge the National Science Foundation for supporting this research under Grant CHE-8807846. We also thank the Rothschild Foundation for a post-doctoral fellowship to E. M. L.

References

1. D. A. Cadenhead in "Structure and Properties of Cell Membranes," G. Benga, ed., Vol. 3, p. 21–63; CRC Press Inc. 1985.
2. a. P. Devaux and H. M. McConnell, *J. Am. Chem. Soc.*, 1972, **99**, 4475. b. E. Sackman and H. Trauble, *J. Am. Chem. Soc.*, 1972, **94**, 4482. c. H. Trauble and E. Sackman, *J. Am. Chem. Soc.*, 1972, **94**, 4499.
3. a. D. Axelrod and D. E. Koppel, J. Schlessinger, E. Elson and W. W. Webb, *Biophys. J.*, 1976, **16**, 1055. b. R. Peters, *Cell Biol. Int. Rep.*, 1981, **5**, 733. c. R. Peter and K. Beck, *Proc. Natl. Acad. Sci. USA*, 1983, **80**, 7183.
4. a. R. J. Cherry, Biochim. *Biophys. Acta*, 1979, **559**, 289. b. W. Vaz, Z. I. Derko and K. A. Jacobson, *Cell Surface Rev.*, 1982, **8**, 83. c. M. Edidin in "Membrane Structure," J. B. Finean and R. H. Michell, eds., Elsevier 1981, Chapter 2, p. 37. d. M. Edidin in "Current Topics in Membranes and Transport," Vol. 29, p. 91, 1987. e. C. G. Wade in "Structure and Properties of Cell Membranes," G. Benga, ed., CRC Press Inc., 1985, Vol. I, p. 51.
5. a. C. J. Miller and M. Majda, *Anal. Chem.*, 1988, **60**, 1168. b. C. Bourdillon and M. Majda, *J. Am. Chem. Soc.*, 1990, **112**, 1795.
6. M.-P. Pileni, A. M. Braun and M. Gratzel, *Photochem. Photobiol.*, 1980, **31**, 423.
7. D. M. Charych and M. Majda, in preparation.
8. C. E. D. Chidsey, B. J. Feldman and R. V. Murray, *Anal. Chem.*, 1986, **58**, 601.
9. C. J. Miller, C. A. Widrig, D. M. Charych and M. Majda, *J. Phys. Chem.*, 1988, **92**, 1928.
10. L. B. Anderson and C. N. Reilley, *J. Electroanal. Chem.*, 1965, **10**, 295.
11. C. A. Widrig, C. J. Miller and M. Majda, *J. Am. Chem. Soc.*, 1988, **110**, 2009.
12. E. B. Troughton, C. D. Bain, G. M. Whitesides, R. G. Nuzzo, D. L. Allara, and M. D. Porter, *Langmuir*, 1988, **4**, 365.
13. A. J. Bard and L. F. Faulkner, "Electrochemical Methods. Fundamentals and Applications," J. Wiley Inc., 1980, Chapter 6, p. 213.
14. M. H. Cohen and D. Turnbull, *J. Chem. Phys.*, 1959, **31**, 1164.